HHS Public Access

Author manuscript

*Nat Commun*. Author manuscript; available in PMC 2015 March 01.

Published in final edited form as:

*Nat Commun*. ; 5: 4776. doi:10.1038/ncomms5776.

# Site-specific mapping and quantification of protein *S*-sulfenylation in cells

**Jing Yang**[1,2], **Vinayak Gupta**[3], **Kate S. Carroll**[3], and **Daniel C. Liebler**[1,2,*]

[1]Departmemt of Biochemistry, Vanderbilt University School of Medicine, Nashville, TN

[2]Jim Ayers Institute for Precancer Detection and Diagnosis, Vanderbilt-Ingram Cancer Center, Vanderbilt University School of Medicine, Nashville, TN 37232-6350

[3]Department of Chemistry, The Scripps Research Institute, Jupiter, FL 33458

## Abstract

Cysteine S-sulfenylation provides redox regulation of protein functions, but the global cellular impact of this transient post-translational modification remains unexplored. We describe a chemoproteomic workflow to map and quantify over 1,000 S-sulfenylation sites on more than 700 proteins in intact cells. Quantitative analysis of human cells stimulated with hydrogen peroxide or epidermal growth factor measured hundreds of site selective redox changes. Different cysteines in the same proteins displayed dramatic differences in susceptibility to *S*-sulfenylation. Newly discovered S-sulfenylations provided mechanistic support for proposed cysteine redox reactions and suggested novel redox mechanisms, including S-sulfenyl-mediated redox regulation of the transcription factor HIF1A by SIRT6. S-sulfenylation is favored at solvent-exposed protein surfaces and is associated with sequence motifs that are distinct from those for other thiol modifications. S-sulfenylations affect regulators of phosphorylation, acetylation and ubiquitylation, which suggests regulatory crosstalk between redox control and signaling pathways.

Protein S-sulfenylation, the reversible oxidation of protein cysteinyl thiols to sulfenic acids (R-SOH), has emerged as a potential mechanism to regulate protein functions, signal transduction and effects of oxidative stress[1]. Because of its intrinsically unstable nature, protein S-sulfenylation previously has been detected indirectly by monitoring loss of reactivity with thiol-modifying reagents[2]. Recently, the use of the β-dicarbonyl compound dimedone and its analogs has enabled selective labeling and detection of protein S-sulfenylation[1]. This strategy has expanded the catalog of proteins that apparently undergo S-sulfenylation. For example, Paulsen et al[3] reported that the use a clickable dimedone-base probe, DYn-2, to detect S-sulfenylated proteins in human cells and demonstrated that a



*Correspondence should be addressed to D.C.L. (daniel.liebler@vanderbilt.edu).

**AUTHOR CONTRIBUTIONS**

J.Y. conceived the project, designed and performed the experiments, analyzed the data, and wrote the manuscript; V.G. synthesized the DYn-2-d6 and contributed related method description; K.S.C. and D.C.L. conceived and directed the project, analyzed the data and edited the manuscript.

**COMPETING FINANCIAL INTERSESTS**

The authors declare no competing financial interests.

critical active site cysteine (Cys797) on the EGF receptor (EGFR) is directly S-sulfenylated by $H_2O_2$ induced through growth factor stimulation. Using the same probe, Kulathu et al.[4] found that many ovarian tumor deubiquitinases undergo S-sulfenylation upon treatment with $H_2O_2$. Leonard et al.[5] used an azide analog of dimedone for selective labeling, capture by Staudinger ligation, and identification of S-sulfenylated proteins in cells by liquid chromatography-tandem mass spectrometry (LC-MS/MS). They identified 193 proteins as apparent targets of protein S-sulfenylation, but no specific sites of modification were reported.

Major limitations of such protein-level identifications are false-positive identifications due to nonspecifically-captured proteins and a lack of information about the sites and multiplicity of redox changes. Only site-specific mapping of S-sulfenylated residues provides definitive confirmation. A method for global identification and quantitation of S-sulfenylated residues would enable comprehensive assessment of this redox modification in cell systems.

We and others have recently reported several chemoproteomic strategies for identifying protein modification sites with various clickable probes (azide or alkyne chemicals)[6–11]. Typically, cells or protein extracts are first labeled with the probe and the labeled proteins then are tagged with a functionalized biotin reagent containing a cleavable linker via $Cu^I$-catalyzed azide-alkyne cycloaddition reaction (CuAAC, click chemistry). After tryptic digestion, modified peptides are enriched by biotin-streptavidin affinity and analyzed by LC-MS/MS. Although it has been applied to analyze protein extracts labeled with probes *in vitro*, this approach has never been optimized for global, site-specific mapping and quantitation of low-abundance chemical modifications in intact cellular systems. This challenge thus presents a barrier to the study of labile redox modifications in cells.

Here we describe use of this selective cysteine sulfenic acid labeling technique in a highly efficient chemoproteomics workflow (Fig. 1a) to globally map the sites of protein S-sulfenylation in cultured cells. The strategy can identify ~1000 protein S-sulfenylation events for a single cellular condition. Moreover, we quantitatively measure hundreds of dynamic cellular S-sulfenylation changes in response to either exogenous $H_2O_2$ or growth factor stimulation. Functional analysis of a novel S-sulfenylated site on SIRT6 protein reveals an unexpected role of this histone deacetylase as a potential redox sensor and transducer. Bioinformatic and structural analyses indicates that protein S-sulfenylation can impact many biological and functional categories and has distinct structural features.

## Results

### Site-specific mapping of protein S-sulfenylation in cells

First, we optimized a method for modified peptide capture based on our previously reported chemoproteomic protocol[6]. The major challenge we faced was to improve the efficiency of click derivatization of DYn-2-labeled peptides. Given the literature precedent of poor performance under aqueous conditions of tris[(1-benzyl-1H-1,2,3-triazol-4-yl)methyl]amine (TBTA), the ligand most widely used for CuAAC acceleration[12], we focused on improvements in the CuAAC reaction to ensure high yields in linking the alkynyl tag to

azido biotinylated peptide. The new protocol has three features: (i) TBTA and the other reagents are dissolved thoroughly in the reaction solvent containing 30% acetonitrile in mild acid, (ii) a high catalyst concentration is used, and (iii) the CuAAC reaction is performed after tryptic digestion and excess biotin reagents are removed by strong cation exchange (SCX). We also optimized the procedures for washing streptavidin-captured peptides to minimize interferences from TBTA and byproducts of CuAAC reaction.

We then used the optimized workflow, termed SulfenM, with a selective cysteine sulfenic acid labeling probe, DYn-2[3], to site-specifically map the sites of protein S-sulfenylation in RKO colon adenocarcinoma cells. We detected 1153 distinct S-sulfenylated peptides (Supplementary Dataset 1) using high energy collisional dissociation (HCD) MS/MS[13] on a Q-Exactive MS instrument, which provides full mass range peptide fragmentation with high mass accuracy, greatly aiding precise identification. The mass errors for the precursor and fragment ions of modified peptides were within the range of 5 ppm and 20 ppm, respectively (Supplementary Fig. 1). In addition, we found that the DYn-2/click-derived modification produced several major diagnostic fragment ions (DFIs) at *m/z* 368.16, 366.15, 336.19 (Fig. 1b), which are generated by fragmentations analogous to those reported for cysteine conjugates[14]. We observed that all HCD spectra of DYn-2/click modified peptides contain DFIs, which increase the confidence of S-sulfenylated peptide identifications. Furthermore, we designed a decision-tree approach for validation of peptide-spectrum matches (PSM) (Supplementary Fig. 2), which yields 952 fully localized S-sulfenylated sites on 680 proteins (Supplementary Dataset 2). We further verified several novel protein targets of S-sulfenylation, including ACTN, ACLY, CFL1 EEF1G, MAPK1, HSP90, RPL18, SIRT6, TUBB and YWAHE by a combination of affinity purification and western blotting (Supplementary Fig.3).

## Quantitative analysis of the S-sulfenylome in cells

Next, we adapted our approach to quantify alterations in global S-sulfenylation in response to stimuli (Fig.2a). In this strategy, termed SulfenQ, cells in two different conditions are labeled with light and heavy DYn-2 isotopomers, then combined and digested with trypsin. Tagged peptides are biotinylated, captured, and enriched as described above. The relative change in protein S-sulfenylation between two conditions is determined by the ratio of extracted ion current peak intensities for heavy and light isotope-labeled DYn-2-tagged peptides, using the MS1 filtering function of Skyline software[15]. We first verified the accuracy of SulfenQ by mixing varying amounts of light or heavy DYn-2 labeled RKO proteomes in different ratios (L:H = 1:4, 1:1, 4:1). The observed signals for labeled S-sulfenylated peptides closely matched the expected ratios (Supplementary Fig. 4).

We measured S-sulfenylation changes produced in RKO cells by the prototypical oxidant hydrogen peroxide ($H_2O_2$), which also plays essential regulatory roles in multiple cellular processes[16]. We observed dramatic changes in the S-sulfenylome upon $H_2O_2$ treatment, with an increase of >2-fold in the intensities of >89% of modified sites (Fig.2b, Supplementary Fig.5 & Supplementary Dataset 3). We also noted that multiple S-sulfenylated sites on the same protein could sense exogenous $H_2O_2$ in a markedly different manner. For example, ratios of $R_{H/L}$ of nine cysteines on fatty acid synthase (FASN)

distributed broadly over a >60-fold range (Fig.2b, Supplementary Fig.6). Of two cysteine residues on PRDX6 (Fig.2c), C91 showed dramatic increase in S-sulfenylation after $H_2O_2$ treatment ($R_{H/L}$ = 9.15), whereas the PRDX6 active site C47 showed opposite behavior ($R_{H/L}$ = 0.07), in agreement with the well-known susceptibility of the active site of this 1-Cys peroxiredoxin to overoxidation (to Cys-$SO_2H$ or Cys-$SO_3H$). Furthermore, changes in S-sulfenylation of two adjacent cysteine residues (C120 and C127, Fig. 2d) on the epidermal fatty acid binding protein FABP5 were also strikingly different in response to $H_2O_2$ (Fig. 2c). C127 was more highly S-sulfenylated after $H_2O_2$ treatment ($R_{H/L}$ = 2.43), whereas S-sulfenylation on C120 remained almost unchanged ($R_{H/L}$ = 0.79). This finding might suggest that S-sulfenylation of C127, rather than C120, was responsible for a disulfide bond formation within the ligand binding cavity of FABP5, which was proposed to be crucial for its biological activity[17].

The foregoing experiments led us to further explore S-sulfenylome changes by cellular $H_2O_2$ production in response to growth factor signaling. Accordingly, we investigated the EGF-dependent changes in protein S-sulfenylation in a global and site-specific manner. As expected, we observed dramatic changes in the S-sulfenylome upon EGF treatment in A431 cells (100 ng/mL, 5 min), with an increase of >2-fold in the intensities of approximately half of the detected sites (Supplementary Fig.7 & Supplementary Dataset 4), whereas the remaining sites were unchanged (0.5<R<2). In contrast, $H_2O_2$ produced significant changes in over 90% of detected S-sulfenyl sites. Although global S-sulfenylation changes induced by EGF correlated well with those produced by exogenous $H_2O_2$ (Fig.2e), the endogenous, EGF-driven oxidative perturbation was considerably more selective and specific. For example, as shown in Fig.2f, S-sulfenylation of two cysteines on CFL1 protein (C139 and C147) was increased by $H_2O_2$ treatment ($R_{H/L}$ = 2.7 and 2.4, respectively), whereas their S-sulfenyl forms were not changed by EGF treatment ($R_{H/L}$ = 1.1 and 0.89, respectively).

Surprisingly, S-sulfenylation of the catalytic C47 residue PRDX6 was unchanged in A431 cells treated with EGF, whereas S-sulfenylation of the catalytic site C100 on the 2-Cys peroxiredoxin PRDX5 was increased 6.9-fold, suggesting that these highly nucleophilic sites are not over-oxidized to sulfinic acid (-$SO_2H$) or sulfonic acid (-$SO_3H$) by endogenous oxidants (Fig.2g). We also observed that 5 min treatment in A431 cells with 100 ng/mL EGF does not induce overoxidation on PRDX1 or PRDX2 (Fig.2h). Since peroxiredoxins maintain control of protein redox homeostasis, their resistance to endogenous oxidant production may confer relative stability of the cellular S-sulfenylome in response to physiologic stimuli.

## Functional analysis of S-sulfenylation on SIRT6

Among the most highly and consistently S-sulfenylated proteins was SIRT6, a member of a conserved family of $NAD^+$-dependent deacetylases with important functions in cellular metabolism, stress resistance, and cancer[18–21] (Fig.3a-b). SIRT6 functions as a corepressor of HIF1A, thereby regulating glucose homeostasis, but the molecular basis of their interaction is still unclear[22]. Among the five cysteine residues on SIRT6, Cys18 was exclusively and highly S-sulfenylated (Supplementary Dataset 2). We thus hypothesized that SIRT6 binds HIF1A in a redox-dependent manner. To test this hypothesis, we incubated

human recombinant SIRT6 with HIF1A protein fragment (530–826), which contains three cysteines, with or without $H_2O_2$. We then analyzed the complexes by electrophoresis and western blotting. Without $H_2O_2$ treatment, SIRT6 migrated as a single band corresponding to its monomeric form (Fig.3c). Upon $H_2O_2$ treatment in the presence of HIF1A, SIRT6 migrated at higher apparent molecular weights, particularly in non-reducing gels (Fig.3c). HIF1A migration displayed similar $H_2O_2$-dependent migration in the presence of SIRT6 (Fig.3c). These results suggested that an intermolecular disulfide bond was formed between SIRT6 and HIF1A. Moreover, treatment with dimedone, a cysteine sulfenic acid labeling reagent, abolished these mobility shifts (Fig.3d), suggesting that this oxidative aggregation is initiated by an S-sulfenylation event. We further analyzed the mixture by LC-MS/MS to identify the specific S-sulfenylation event on SIRT6 responsible for intermolecular disulfide bond formation between SIRT6 and HIF1A. An ion with a mass matching the theoretical mass of disulfide-linked peptides 18–24 of SIRT6 and 799–810 of HIF1A was detected (Fig. 3e, inset). MS/MS fragmentation of this peptide ion further confirmed the expected SIRT6 and HIF1A sequences (Fig.3e). Taken together, these data establish that the SIRT6-HIF1A disulfide linkage is formed between Cys18 (SIRT6) and Cys800 (HIF1A) (Fig.3f) and is mediated by cysteine S-sulfenylation. This result suggests that SIRT6 may exert redox control of HIF1A transcriptional activity through reversible formation of disulfide-linked SIRT6-HIF1A complex.

## Bioinformatics analysis of the S-sulfenylome

To better understand the systems impact of protein S-sulfenylation, we used DAVID software[23] to perform several bioinformatics enrichment analyses of the S-sulfenylome detected in RKO cells. S-sulfenylated proteins are widely distributed across all major cellular compartments (Fig.4a) and represent diverse cellular processes and pathways (Fig. 4b). A large number of S-sulfenylated proteins are present in the nucleus (Fig.4a) and represent most major nuclear processes, including RNA processing, translation, transportation, and cell cycle (Fig.4b). We did not detect S-sulfenylation of redox-sensitive transcription factors, which are believed to function as the important determinants of proper redox state in the nucleus[24]. This may reflect the low abundance of many transcription factors, such that detection of their S-sulfenyl peptides is suppressed by the presence of more abundant S-sulfenyl peptides. In addition, extensively S-sulfenylated nuclear proteins, such as EEF1A1, NTMT1, and SIRT6 may function as $H_2O_2$ sensors that then interact with transcription factors, thus enabling redox-regulation through thiol-disulfide exchange, rather than direct oxidation by $H_2O_2$[25].

GO classification and KEGG pathway analysis revealed enrichment of S-sulfenylated proteins involved in protein deubiquitination (GO_BP, $p = 9.1\times10^{-9}$; GO_MF, $p = 2.9\times10^{-3}$; KEGG, $p = 1.8\times10^{-2}$). Together with recent studies that show deubiquitinases can be targeted and regulated by S-sulfenylation[4, 26], these findings strongly suggest that protein ubiquitination may be influenced by redox regulation.

We also noted that S-sulfenylated proteins were enriched in several biological processes and pathways involving cell metabolism, including glucose catabolic processes (GO_BP, $p = 3.2\times10^{-4}$), glycolysis (KEGG, $p = 4.5\times10^{-2}$), pentose phosphate pathway (KEGG, p =

$4.6\times10^{-2}$), and fatty acid metabolism (KEGG, $p = 6.6\times10^{-2}$). In particular, pyruvate kinase M2 (PKM2), a glycolytic enzyme, was S-sulfenylated on three cysteine residues (C49, C358, and C423/424) under basal conditions. One of these (C358) was found to be critical for metabolic reprogramming regulated by PKM2 *via* reversible oxidation during cancer development[27]. In another example, S-sulfenylation of C212 on fatty acid synthase (FASN) may drive intra-molecular disulfide formation in the β-ketoacyl synthase domain, thereby blocking the active site (C161) for fatty acid synthesis (Supplementary Fig. 6)[28].

## Structure profiling of S-sulfenylated cysteine residues

We identified a total of 1105 S-sulfenylated sites on 778 proteins in RKO cells, the majority of which (92%) had only one or two S-sulfenylated residues (Fig.5a). A few proteins (1.3%) were extensively oxidized (number of sites ≥ 5), including FASN and MKI67, both with 9 S-sulfenyl sites. We explored structural properties of the modified cysteine residues with several computational tools and available crystal structures. First, we performed a prediction analysis of the relative residue surface accessibility (RSA) for all cysteine residues (modified and un-modified) within the S-sulfenylome using NetSurfP[29]. As expected, >60% of the S-sulfenylated cysteine residues were solvent-exposed (with a relative RSA of greater than 25%), which was dramatically higher than that (<30%) for all unmodified cysteine residues within the same proteins. We also compared the probability distribution for relative RSA for S-sulfenylated cysteines with that for unmodified cysteine residues (Fig. 5b) and by plotting the percentile rankings against each other (Fig. 5c). Both analyses demonstrated that S-sulfenylated cysteine residues showed a marked tendency to reside on surface-accessible areas compared to unmodified cysteine residues, which suggests that solvent accessibility is one of the major determinants for the redox reactivity of cysteines.

To further confirm this finding, we mapped identified S-sulfenylated sites onto several proteins with available crystal structures and calculated solvent accessibilities with a default probe radius of 1.4 Å. For example, among four cysteines on human CFL1, only two highly solvent-accessible residues, C139 and C147 (Fig. 5d), were found to be targeted by S-sulfenylation under both basal and stimulated conditions. In another example, the highly exposed catalytic cysteine residue, C152, of GAPDH also was highly S-sulfenylated, even under basal oxidation conditions (Supplementary Fig. 8). However, S-sulfenylation of C247, one of the buried cysteine residues within GAPDH, was still detectable, although much less abundant (Supplementary Fig. 8), in accordance with an earlier study of thiol reactivity in GAPDH[30]. We should note that detection of S-sulfenylation requires that our probe be able to react with the oxidized residue and that steric features may hinder labeling of some S-sulfenylated cysteines. Accordingly, our conclusion regarding the potential surface-localization tendency of S-sulfenylation may be biased somewhat by an unavoidable limitation of chemical labeling strategy.

To further explore structural features that may define protein S-sulfenylation, we examined flanking sequences of S-sulfenylated cysteine residues with the pLogo algorithm for the presence of linear motifs and we further compared these to motifs associated with other cysteine modifications, such as S-nitrosylation[31] and electrophile-based alkylation[7]. Strikingly, S-sulfenylated cysteines resided within consensus motifs with features distinct

from those for S-nitrosylated and electrophile-sensitive cysteines. Specifically, Glu was significantly overrepresented at the −4, −3, +1, +3, +4, and +5 position of S-sulfenylation sites, whereas Lys was significantly overrepresented at the −6, −5, −2, and +6 position ($p < 0.05$, Fig. 6). Notably, Glu and Lys have complementary physiochemical properties (Glu is negatively charged and acts as a hydrogen acceptor, whereas Lys is a positively charged and acts as a hydrogen donor). Protonated Glu may be capable of reducing the pKa of an adjacent thiol *via* hydrogen bond formation[32]. Glu was highly represented in the +3 and +4 positions of S-sulfenylated sites (Fig. 6) and is also highly conserved at the +3 position adjacent to the catalytic cysteines of all the 2-Cys peroxiredoxins, the best-known targets of $H_2O_2$. We also found that Cys is largely absent in consensus flanking sequences of all the aforementioned cysteine modifications (Fig. 6). Indeed, the absence of adjacent cysteines is considered to be the major stabilizing factor for cysteine sulfenic acid[33].

## Discussion

Here we describe a highly efficient chemoproteomics platform, which we applied to quantitative S-sulfenylome analysis in intact cells. In total, we identified over 1000 S-sulfenylation sites on more than 700 proteins (Supplementary Datasets 2–4), which demonstrates the potential of this platform for further systematic study of biologically relevant S-sulfenylation events. To our knowledge, the current dataset encompasses most known S-sulfenylated sites and proteins in mammalian cells and expands by two orders of magnitude the number of such sites previously listed in Uniprot. The use of DFI in MS/MS spectra and our decision-tree validation procedure ensures that these site assignments are of high reliability. Although the DYn-2 probe labeled diverse sequences, there are limitations to the labeling approach. Some S-sulfenylated cysteines may be inaccessible to the DYn-2 probe for steric reasons or because rapid formation of intramolecular bonds, such as disulfide (e.g., 2-Cys PRDXs) and sulfenylamide[34] (e.g., PTP1B) blocks reaction of DYn-2 with transient sulfenic acids in these proteins. A particularly important aspect of our approach is that we achieve site-specific mapping of large numbers of modifications in intact cells. Most previous studies of cysteinyl modifications were done with cell lysates treated with much higher concentrations of thiol-modifying agents[35–37]. A key assumption in S-sulfenylation analysis by DYn-2 labeling is that the 2h probe labeling treatment itself does not induce oxidative stress sufficient to perturb cellular redox state. This has been established by previous experiments, which demonstrated that DYn-2 does not alter cell viability, glutathione redox balance or generate reactive oxygen species under the same labeling conditions described here[3]. Moreover, DYn-2 labeling does not result in overoxidation of peroxiredoxins (Supplementary Fig. 9).

Some recently published reports revealed that biological functions of a few proteins, such as cofilin 1 (CFL1)[38], pyruvate kinase M2 (PKM2)[27], and superoxide dismutase 1(SOD1)[39] can be regulated by redox reactions, which were interpreted as reversible cysteine oxidations. Our identification of specific S-sulfenylation sites on these proteins provides further support for this hypothesis. For instance, of four cysteine residues on human CFL1, only C139 and C147 were found to be sensitive to oxidative stress and responsible for CFL1-induced mitochondrial damage[38]. We detected S-sulfenylation of only these two cysteines on CFL1 protein and also confirmed these by an orthogonal approach

(Supplementary Fig. 3d-e). In addition, functional analysis of a novel S-sulfenylated site at SIRT6 C18, near the N-terminus of the protein, revealed a redox-dependent mechanism for interaction between SIRT6 and the transcriptional factor HIF1A (Fig. 3).

We found S-sulfenylated sites on the functional domains of protein kinases, phosphatases, acetyltransferases, deacetylases, and deubiquitinases (Fig. 4c), suggesting the possibility of regulatory cross-talk between S-sulfenylation and other major posttranslational modification events. Indeed, other recent studies suggest the potential regulatory impact of reversible cysteine oxidation on protein phosphorylation[3, 40], acetylation[41], and ubiquitylation[4, 26, 42]. In addition, gene ontology annotations show that these S-sulfenylated proteins are present in all major cellular compartments and are involved in various biological processes such as cell signaling, response to stress, cell cycle, and cell death (Fig. 4). Structural analysis revealed consensus motifs for S-sulfenylation, such as CxxE, CxxxE, and KxC, and that S-sulfenylation is favored on protein surfaces (Fig. 5–6). In addition to p*K*a, other structural features influencing the local stereoelectronic environment of cysteine residues may direct S-sulfenylation site specificity *in vivo*.

The application of quantitative S-sulfenylome analysis enabled us to quantify exogenous oxidant or growth factor induced redox events in eukaryotic cells in a global and unbiased manner. The strategy we describe here should enable more comprehensive assessment of dynamic S-sulfenylation in different contexts, such as redox perturbations associated with cell signaling, metabolism, inflammation and disease processes. Moreover, adaptation of SulfenQ could enable absolute measurement of protein S-sulfenylation stoichiometry. More broadly, application of our optimized peptide-capture method with other clickable chemical probes should dramatically improve site-specific characterization of other proteomic characteristics and targets. Our analysis platform should thus find broad applications in both chemical biology and drug discovery[43].

## METHODS

### Reagents

Azido-tagged biotin with or without a photocleavable linker (biotin-UV-azide and biotin-azide) were provided by Professor Ned A. Porter [6] (Supplementary Figure 10). The synthesis of these reagents is described in the Supplementary Material of Reference 6. DYn-2 was purchased from Cayman chemicals. DYn-2-d6 was synthesized as described in the Supplementary Methods. Strong cation exchange (SCX) spin columns were purchased from Nest group. Streptavidin sepharose was purchased from GE Healthcare Life Sciences. HPLC-grade water, acetonitrile (ACN), and methanol were purchased from J.T.Baker. Other chemicals and reagents were obtained from Sigma unless otherwise indicated. Antibodies against ACLY (ab40793, diluted at 1:5000), ACTN (ab6276, diluted at 1:5000), CFL1 (ab42824, diluted at 1:1000), EEF1G (ab72368, diluted at 1:5000), MAPK1/ERK2 (ab124362, diluted at 1:1000), RPL18 (ab166711, diluted at 1:1000), SIRT6 (ab88494, diluted at 1:2500), TUBB (ab7792, diluted at 1:5000), PRDX-$SO_{2/3}$H (ab16830, diluted at 1:2000), PRDX1 (ab15571, diluted at 1:2000), and PRDX2 (ab15572, diluted at 1:2000) were purchased from Abcam. Antibodies against HSP90 (CS#4874S, diluted at 1:1000) and

YWAHE/14-3-3ε (CS#9635S, diluted at 1:1000) were purchased from Cell Signaling Technology.

### Cell culture and *in situ* labeling of S-sulfenylated proteins

Human RKO and A431 cells (ATCC) were maintained at 37 °C in a 5% $CO_2$, humidified atmosphere and were cultured in McCoy medium (Invitrogen) and DMEM medium (Invitrogen), respectively, containing 10% FBS (Invitrogen). For qualitative S-sulfenylome analysis, cells were grown until 70–80% confluent, rinsed with PBS quickly, and labeled according to a modification of a recently published protocol[44]. In brief, cells were lifted with 0.25% trypsin-EDTA (Invitrogen), harvested by centrifugation at 1,500×g for 3 min, washed, and resuspended in serum-free McCoy medium at a density of ~5× $10^6$ cells/mL. Intact cells in suspension were incubated with 5 mM sulfenic acid labeling reagent (DYn-2 in DMSO, 2% v/v) at 37°C with rotation. After 2h incubation, cells were collected and washed with cold PBS three times. For quantitative S-sulfenylome analysis of both RKO and A431 cells, the cells were cultured as above, rinsed with PBS quickly and placed overnight in medium without serum. After serum deprivation, RKO cells were treated with the 500 μM $H_2O_2$ or vehicle for 5 min. A431 cells were treated with 100 ng/mL EGF or vehicle for 10 min. Treatments were stopped by removing the medium. Cells treated with and without stimulus then were labeled with DYn-2-*d*6 and DYn-2, respectively For RKO cells, labeling was for 2h; for A431 cells, labeling was for 1h. The resulting cells were routinely examined using a TC-10 automatic cell counter (Bio-Rad) and uniformly showed greater than 95% viability after either stimuli treatment and/or probe labeling. No evidence of oxidative stress in the tested cell lines was observed during the *in situ* chemical labeling, in accord with our recently published studies [3, 5, 45, 46].

### Sample preparation

Cell pellets were lysed on ice in HEPES lysis buffer (50 mM HEPES, 150 mM NaCl, 1% Igepal, pH 7.5) containing 8 mM dithiothreitol (DTT) (Research Products International). The lysate was further incubated at 75°C for 15 min to reduce the reversibly oxidized cysteines. Reduced cysteines then were alkylated with 32 mM iodoacetamide for 30 min in the dark. Protein concentrations of lysate samples were determined with the BCA assay (Pierce Thermo Fisher). For a typical qualitative S-sulfenylome analysis, ~30 mg protein was used. For a quantitative S-sulfenylome analysis, 7.5 mg light- or heavy DYn-2 labeled protein samples were combined. Protein precipitation was performed with a methanol-chloroform system (aqueous phase/methanol/chloroform, 4:4:1 (v/v/v)) [47]. Proteins were collected at the aqueous/organic phase interface as a solid disk after centrifugation at 1,400×g for 20 min at 4°C. Liquid layers were discarded and the protein was washed twice in methanol/chloroform (1:1, v/v), followed by centrifugation at 16,000×g for 10 min at 4 °C to repellet the protein. The protein pellets were evaporated to dryness under vacuum and resuspended with 50 mM ammonium bicarbonate containing 0.2 M urea at a protein concentration of 2 mg/mL. Resuspended proteins were first digested with sequencing grade trypsin (Promega) at a 1:50 (enzyme/substrate) ratio overnight at 37°C. A secondary digestion was performed by adding additional trypsin to a 1:100 (enzyme/substrate) ratio, followed by incubation at 37°C for additional 4 h. The tryptic digests were desalted with

HLB extraction cartridges (Waters). The desalted samples were then evaporated to dryness under vacuum.

### Click chemistry, capture and enrichment

Desalted tryptic digests were reconstituted in a solution containing 30% acetonitrile (ACN), 0.8 mM biotin-UV-azide, 8 mM sodium ascorbate, 1 mM TBTA, and 8 mM $CuSO_4$, pH 6. The pH of the reaction mixture was adjusted using pH-indicator strips and the mixture was incubated for 2h at room temperature with in the dark rotation. The excess biotin reagents were removed by strong cation exchange (SCX) chromatography, as previously reported[48]. In brief, the sample was diluted into SCX loading buffer (5 mM $KH_2PO_4$, 25% acetonitrile, pH 3.0), passed through the SCX spin columns, and washed with several column volumes of loading buffer. The retained peptides were eluted with a series of high-salt buffers containing 100, 200, and 400 mM NaCl. Eluent was diluted 10X with 50 mM sodium acetate buffer (NaAc, pH 4.5) and then allowed to interact with pre-washed streptavidin sepharose for 2 h at room temperature. Streptavidin sepharose then was washed with 50 mM NaAc, 50 mM NaAc containing 2 M NaCl, and water twice each with votexing and/or rotation to remove non-specific binding peptides, and resuspended in 25 mM ammonium bicarbonate. The suspension of streptavidin sepharose was transferred to several glass tubes (VWR), irradiated with 365 nm UV light (Entela, Upland, CA) for 2 h at room temperature with stirring. The supernatant was collected, evaporated to dryness under vacuum, and stored at −20°C until analysis.

### Liquid chromatography-tandem mass spectrometry (LC-MS/MS)

LC-MS/MS analyses were performed on a Q Exactive hybrid quadrupole-Orbitrap mass spectrometer (Thermo Fisher Scientific) operated with an Easy-nLC1000 system (Thermo Fisher Scientific). Samples were reconstituted in 0.1% formic acid and pressure-loaded onto a 360 μm outer diameter × 75 μm inner diameter microcapillary precolumn packed with Jupiter C18 (5 μm, 300 Å, Phenomenex) and then washed with 0.1% acetic acid. The precolumn was connected to a 360 μm outer diameter × 50 μm inner diameter microcapillary analytical column packed with the ReproSil-Pur C18-AQ (3 μm, 120 Å, Dr. Maisch) and equipped with an integrated electrospray emitter tip. The spray voltage was set to 1.5 kV and the heated capillary temperature to 250°C. For qualitative analysis, two different LC gradient conditions were used. Gradient A consisted of 0–15 min, 2% B; 35 min, 15% B; 40 min, 20% B; 50 min, 30% B; 55 min, 35% B; 59–65 min, 90% B; 80–85 min, 2% B (A = water, 0.1% formic acid; B = acetonitrile/0.1% formic acid) at a flow rate of 300 nL/min. Gradient B consisted of 0–10 min, 5% B; 100 min, 35% B; 120–130 min, 90% B; 140–150 min, 5% B at a flow rate of 300 nL/min. For quantitative analysis, gradient A was used to achieve better peak shapes. HCD MS/MS spectra were recorded in the data-dependent mode using a Top 12 method for qualitative analysis and Top 20 method for quantitative analysis, respectively. MS1 spectra were measured with a resolution of 70,000, an AGC target of 3e6, and a mass range from *m/z* 300 to 1800. HCD MS/MS spectra were acquired with a resolution of 17,500, an AGC target of 2e5, and normalized collision energy of 28. Peptide *m/z* that triggered MS/MS scans were dynamically excluded from further MS/MS scans for 20 s. The HCD MS/MS spectra for all identified peptides are provided as Supplementary Dataset 5 and all the raw data files are available for download at both the University of

California at San Diego MassIVE portal (ftp://MSV000078777@massive.ucsd.edu/) and the National Cancer Institute Clinical Proteomic Tumor Analysis Consortium Data Portal (https://cptac-data-portal.georgetown.edu/cptacPublic/). .

## Peptide identification and site localization

Raw data files were analyzed by using TagRecon algorithm[49] (Version 1.4.47) against a decoy protein database consisting of forward and reversed human RefSeq database (Version 20130621). Precursor ion mass tolerance was 0.01 Da, and fragmentation tolerance was 0.1 Da for the database search. The maximum number of modifications allowed per peptide was three, as was the maximum number of missed cleavages allowed. Methionine oxidation (15.9949 Da) and cysteine modifications either by iodoacetamide (carbamidomethyl, 57.0214 Da) or by S-sulfenylcysteine tagged with DYn-2-triazohexanoic acid group (DTH, Figure 1b, 333.1689 Da) were searched as dynamic modifications. For quantitative S-sulfenylome analysis, the heavy DTH modification on cysteine (DTH-*d*6, 339.2065) was also included as dynamic modification during database searching. The maximum Q value of peptide-spectrum matches (PSMs) was adjusted to achieve either a peptide or a protein false discovery rate (FDR) no greater than 5% using IDPicker software (Version 3.0.529) [50]. Because identifications based on one peptide per protein were permitted, a streamlined manual validation approach was used to establish peptide identification and site localization (Supplemental Figure 2). First, the modified peptides whose matched spectra did not contain the major three diagnostic fragment ions (*m/z* 368.16, 366.15, and 336.19) were excluded from further consideration. MS/MS spectra of identified S-sulfenylated peptides then were annotated automatically with the SeeMS tool embedded in IDPicker software. The mass errors of the annotated peaks were required to be less than 20 ppm. All the automatically annotated spectra were manually evaluated according a previously published protocol for verification of automated peptide identification[51]. For identified peptides containing more than one cysteine residue, at least three DTH modification-specific fragment ions were required for unambiguous site localization. PSMs with ambiguously localized sites identified with proper peak annotation also were retained in the final dataset.

## Quantitative analysis

For quantitative S-sulfenylome analysis, database search results were processed using Skyline software[52] according to the tutorial for MS1 full-scan filtering (https://skyline.gs.washington.edu/labkey/wiki/home/software/Skyline/page.view?name=tutorial_ms1_filtering). In brief, Skyline spectral libraries were generated from database searches (as described above) of the raw data files. A subset FASTA database containing all the identifications (with and/or without modification) exported from the IDPicker files then was imported into Skyline. The peptide list was further refined in Skyline by removing all unmodified peptides, as well as modified peptides with incorrect annotations. Raw files then were directly imported into Skyline in their native file format[53]. Because MS/MS spectra were obtained in data-dependent acquisition mode, peptides were not always identified by a peptide-spectrum match (PSM) in every replicate or run. In cases where a probe-modified peptide was identified in one run, but not in another, several criteria were applied to identify the corresponding peak in the run without the peptide identification. First, the retention time of the PSM-identified peptide (indicated by ID, Supplementary

Figure 4–5) was used to position a retention time window (± 3 min) across the run lacking the same peptide identification. Second, the resolution for extracting the MS1 filtering chromatogram of the target precursor ions with both light and heavy labeled peptides was set to 70,000 at 400 Th. The use of a deuterated probe could further complicate the analysis, since there is a slight difference in the elution times of light- and deuterated (heavy, *d*6)-tagged peptide pairs, with the deuterated isotopomer eluting 1–2 s before the light analog. After data import, therefore, graphical displays of chromatographic traces for the top three isotopic peaks were manually inspected for proper peak picking of MS1 filtered peptides; those with isotopic dot product scores lower than 0.8 were rejected to ensure that the correct peak pairs were identified. Pairs with isotopic dot product scores lower than 0.8 were rejected to further ensure the correct identification of peak pairs. In addition, several criteria were used to ensure the high accuracy of quantification: 1) signal to noise (S/N) of all the detected peptides was required to be higher than five; (2) baseline separation was required between the isotopic peaks of a quantifiable peptide and unknown isobaric interference; (3) manual integration was applied if necessary. Only the most abundant isotope for each peptide was used for quantitation. Following data extraction, the ratios of peptide areas of heavy DTH adducts to their light isotopomers ($R_{H:L}$) were calculated automatically. Quantitation results were obtained from three biological replicates with two LC-MS/MS runs for each. All details for peptide quantitation using Skyline MS1 filtering are provided in Supplementary Dataset 3–4.

## Bioinformatics

Relative residue surface accessibility (RSA) information was obtained with the prediction algorithm NetSurfP[29] (Version 1.1). AQ-Q plot was used to determine if there was enrichment for exposed or buried cysteines for S-sulfenylated versus unmodified cysteines. The consensus sequence motifs of S-sulfenylated cysteines were visualized by pLogo[54], a linear sequence prediction algorithm based on their statistical significance ($p < 0.05$). The crystal structures of FABP5, CFL1, GAPDH, and FASN were visualized by Discovery Studio (Version 2.5, Accelrys) and the relative RSA values for cysteine residues were calculated with a default probe radius of 1.4 Å. Gene Ontology (GO) and KEGG pathway enrichment ($p < 0.05$) analyses were performed by using the functional annotation tool DAVID[23].

## Affinity purification and western blotting

RKO cells were cultured, treated with or without $H_2O_2$, and labeled with DYn-2 as described above. Cells were lysed in HEPES lysis buffer in the presence of 200 unit/mL catalase (Sigma). Cell lysate (2 mg/mL, 1 mL) was incubated with 100 μM azido-tagged biotin with a photocleavable linker, 1 mM sodium ascorbate, 100 μM TBTA, and 1 mM $CuSO_4$ for 2 h in the dark at room temperature with rotation. The proteins were precipitated with chloroform/methanol system as described above. The resulting protein precipitate then was resolubilized and subjected to streptavidin pull-down. After 1.5 h incubation at room temperature, beads were washed with 1% SDS (x2), 4M urea (x2), 1M NaCl (x1), and $H_2O$ (x2). Beads then were resuspended in 25 mM ammonium bicarbonate buffer and subjected to UV photorelease as described above. The collected proteins were resolved on SDS-PAGE

gels and immunoblotted with antibodies as indicated. Detection was performed with the Odyssey Infrared Imaging System (Li-Cor).

Alternatively, cell lysates (1 mg protein) were incubated with 2 μg antibodies overnight at 4 °C. The immune-complex then was treated with 20 μL protein A/G plus agarose (Pierce) and incubated for 1h at 4 °C. The mixture was washed three times with IP lysis/wash buffer (Pierce) and PBS once. To analyze immunoprecipitated proteins, the beads were treated with 30 μl click chemistry mix (100 μM Azido-tagged biotin without photocleavable linker, 1 mM sodium ascorbate, 100 μM TBTA, 1 mM $CuSO_4$ in PBS). Reactions were quenched by boiling with 15 μL LDS sample buffer (Life Technologies) for 10 min. The collected proteins were analyzed as above except that the DYn-2-labeled protein was detected by fluorescent conjugated streptavidin (Life Technologies) and immunoblotting as described above.

## Supplementary Material

Refer to Web version on PubMed Central for supplementary material.

## ACKNOWLEDGEMENTS

We thank Keri Tallman and Ned Porter for the azido tagged biotin reagents, Lisa Zimmerman and Kristin Carpenter for assistance with LC-MS/MS, Hye-Young Kim, De Lin and Simona Codreanu for helpful discussions. This work was supported by NIH grants U24CA159988 and GM102187.

## REFERENCES

1. Paulsen CE, Carroll KS. Cysteine-mediated redox signaling: chemistry, biology, and tools for discovery. Chem Rev. 2013; 113:4633–4679. [PubMed: 23514336]
2. Leonard SE, Carroll KS. Chemical 'omics' approaches for understanding protein cysteine oxidation in biology. Curr Opin Chem Biol. 2011; 15:88–102. [PubMed: 21130680]
3. Paulsen CE, et al. Peroxide-dependent sulfenylation of the EGFR catalytic site enhances kinase activity. Nat Chem Biol. 2012; 8:57–64. [PubMed: 22158416]
4. Kulathu Y, et al. Regulation of A20 and other OTU deubiquitinases by reversible oxidation. Nat Commun. 2013; 4:1569. [PubMed: 23463012]
5. Leonard SE, Reddie KG, Carroll KS. Mining the thiol proteome for sulfenic acid modifications reveals new targets for oxidation in cells. ACS Chem Biol. 2009; 4:783–799. [PubMed: 19645509]
6. Kim HY, Tallman KA, Liebler DC, Porter NA. An azido-biotin reagent for use in the isolation of protein adducts of lipid-derived electrophiles by streptavidin catch and photorelease. Mol Cell Proteomics. 2009; 8:2080–2089. [PubMed: 19483245]
7. Weerapana E, et al. Quantitative reactivity profiling predicts functional cysteines in proteomes. Nature. 2010; 468:790–795. [PubMed: 21085121]
8. Wang C, Weerapana E, Blewett MM, Cravatt BF. A chemoproteomic platform to quantitatively map targets of lipid-derived electrophiles. Nat Methods. 2014; 11:79–85. [PubMed: 24292485]
9. Szychowski J, et al. Cleavable biotin probes for labeling of biomolecules via azide-alkyne cycloaddition. J Am Chem Soc. 2010; 132:18351–18360. [PubMed: 21141861]
10. Qian Y, et al. An isotopically tagged azobenzene-based cleavable linker for quantitative proteomics. Chembiochem. 2013; 14:1410–1414. [PubMed: 23861326]
11. Zheng T, Jiang H, Wu P. Single-stranded DNA as a cleavable linker for bioorthogonal click chemistry-based proteomics. Bioconjug Chem. 2013; 24:859–864. [PubMed: 23627610]

12. Presolski SI, Hong V, Cho SH, Finn MG. Tailored ligand acceleration of the Cu-catalyzed azide-alkyne cycloaddition reaction: practical and mechanistic implications. J Am Chem Soc. 2010; 132:14570–14576. [PubMed: 20863116]
13. Olsen JV, et al. Higher-energy C-trap dissociation for peptide modification analysis. Nat Methods. 2007; 4:709–712. [PubMed: 17721543]
14. Levsen K, et al. Structure elucidation of phase II metabolites by tandem mass spectrometry: an overview. J Chromatogr A. 2005; 1067:55–72. [PubMed: 15844510]
15. Schilling B, et al. Platform-independent and label-free quantitation of proteomic data using MS1 extracted ion chromatograms in skyline: application to protein acetylation and phosphorylation. Mol Cell Proteomics. 2012; 11:202–214. [PubMed: 22454539]
16. Veal EA, Day AM, Morgan BA. Hydrogen peroxide sensing and signaling. Mol Cell. 2007; 26:1–14. [PubMed: 17434122]
17. Hohoff C, Borchers T, Rustow B, Spener F, van Tilbeurgh H. Expression, purification, and crystal structure determination of recombinant human epidermal-type fatty acid binding protein. Biochemistry. 1999; 38:12229–12239. [PubMed: 10493790]
18. Mostoslavsky R, et al. Genomic instability and aging-like phenotype in the absence of mammalian SIRT6. Cell. 2006; 124:315–329. [PubMed: 16439206]
19. Sebastian C, et al. The histone deacetylase SIRT6 is a tumor suppressor that controls cancer metabolism. Cell. 2012; 151:1185–1199. [PubMed: 23217706]
20. Toiber D, et al. SIRT6 recruits SNF2H to DNA break sites, preventing genomic instability through chromatin remodeling. Mol Cell. 2013; 51:454–468. [PubMed: 23911928]
21. Kugel S, Mostoslavsky R. Chromatin and beyond: the multitasking roles for SIRT6. Trends Biochem Sci. 2014; 39:72–81. [PubMed: 24438746]
22. Zhong L, et al. The histone deacetylase Sirt6 regulates glucose homeostasis via Hif1alpha. Cell. 2010; 140:280–293. [PubMed: 20141841]
23. Huang da W, Sherman BT, Lempicki RA. Systematic and integrative analysis of large gene lists using DAVID bioinformatics resources. Nat Protoc. 2009; 4:44–57. [PubMed: 19131956]
24. Ushio-Fukai M. Localizing NADPH oxidase-derived ROS. Sci STKE. 2006; 2006:re8. [PubMed: 16926363]
25. Delaunay A, Pflieger D, Barrault MB, Vinh J, Toledano MB. A thiol peroxidase is an H2O2 receptor and redox-transducer in gene activation. Cell. 2002; 111:471–481. [PubMed: 12437921]
26. Lee JG, Baek K, Soetandyo N, Ye Y. Reversible inactivation of deubiquitinases by reactive oxygen species in vitro and in cells. Nat Commun. 2013; 4:1568. [PubMed: 23463011]
27. Anastasiou D, et al. Inhibition of pyruvate kinase M2 by reactive oxygen species contributes to cellular antioxidant responses. Science. 2011; 334:1278–1283. [PubMed: 22052977]
28. Pappenberger G, et al. Structure of the human fatty acid synthase KS-MAT didomain as a framework for inhibitor design. J Mol Biol. 2010; 397:508–519. [PubMed: 20132826]
29. Petersen B, Petersen TN, Andersen P, Nielsen M, Lundegaard C. A generic method for assignment of reliability scores applied to solvent accessibility predictions. BMC Struct Biol. 2009; 9:51. [PubMed: 19646261]
30. Seo YH, Carroll KS. Quantification of protein sulfenic acid modifications using isotope-coded dimedone and iododimedone. Angew Chem Int Ed Engl. 2011; 50:1342–1345. [PubMed: 21290508]
31. Doulias PT, Tenopoulou M, Greene JL, Raju K, Ischiropoulos H. Nitric oxide regulates mitochondrial fatty acid metabolism through reversible protein S-nitrosylation. Sci Signal. 2013; 6:rs1. [PubMed: 23281369]
32. Witt AC, et al. Cysteine pKa depression by a protonated glutamic acid in human DJ-1. Biochemistry. 2008; 47:7430–7440. [PubMed: 18570440]
33. Gupta V, Carroll KS. Sulfenic acid chemistry, detection and cellular lifetime. Biochim Biophys Acta. 2013
34. van Montfort RL, Congreve M, Tisi D, Carr R, Jhoti H. Oxidation state of the active-site cysteine in protein tyrosine phosphatase 1B. Nature. 2003; 423:773–777. [PubMed: 12802339]

35. Rosenwasser S, et al. Mapping the diatom redox-sensitive proteome provides insight into response to nitrogen stress in the marine environment. Proc Natl Acad Sci U S A. 2014; 111:2740–2745. [PubMed: 24550302]
36. Brandes N, et al. Time line of redox events in aging postmitotic cells. Elife. 2013; 2:e00306. [PubMed: 23390587]
37. Su D, et al. Proteomic identification and quantification of S-glutathionylation in mouse macrophages using resin-assisted enrichment and isobaric labeling. Free Radic Biol Med. 2014; 67:460–470. [PubMed: 24333276]
38. Klamt F, et al. Oxidant-induced apoptosis is mediated by oxidation of the actin-regulatory protein cofilin. Nat Cell Biol. 2009; 11:1241–1246. [PubMed: 19734890]
39. Juarez JC, et al. Superoxide dismutase 1 (SOD1) is essential for H2O2-mediated oxidation and inactivation of phosphatases in growth factor signaling. Proc Natl Acad Sci U S A. 2008; 105:7147–7152. [PubMed: 18480265]
40. Woo HA, et al. Inactivation of peroxiredoxin I by phosphorylation allows localized H(2)O(2) accumulation for cell signaling. Cell. 2010; 140:517–528. [PubMed: 20178744]
41. Hwang JW, Yao H, Caito S, Sundar IK, Rahman I. Redox regulation of SIRT1 in inflammation and cellular senescence. Free Radic Biol Med. 2013; 61C:95–110. [PubMed: 23542362]
42. Cotto-Rios XM, Bekes M, Chapman J, Ueberheide B, Huang TT. Deubiquitinases as a signaling target of oxidative stress. Cell Rep. 2012; 2:1475–1484. [PubMed: 23219552]
43. Simon GM, Niphakis MJ, Cravatt BF. Determining target engagement in living systems. Nat Chem Biol. 2013; 9:200–205. [PubMed: 23508173]
44. Truong TH, Carroll KS. Bioorthogonal chemical reporters for analyzing protein sulfenylation in cells. Curr Protoc Chem Biol. 2012; 4:101–122.
45. Depuydt M, et al. A periplasmic reducing system protects single cysteine residues from oxidation. Science. 2009; 326:1109–1111. [PubMed: 19965429]
46. Reddie KG, Seo YH, Muse Iii WB, Leonard SE, Carroll KS. A chemical approach for detecting sulfenic acid-modified proteins in living cells. Mol Biosyst. 2008; 4:521–531. [PubMed: 18493649]
47. Hulce JJ, Cognetta AB, Niphakis MJ, Tully SE, Cravatt BF. Proteome-wide mapping of cholesterol-interacting proteins in mammalian cells. Nat Methods. 2013; 10:259–264. [PubMed: 23396283]
48. Alfaro JF, et al. Tandem mass spectrometry identifies many mouse brain O-GlcNAcylated proteins including EGF domain-specific O-GlcNAc transferase targets. Proc Natl Acad Sci U S A. 2012; 109:7280–7285. [PubMed: 22517741]
49. Dasari S, et al. TagRecon: high-throughput mutation identification through sequence tagging. J Proteome Res. 2010; 9:1716–1726. [PubMed: 20131910]
50. Ma ZQ, et al. IDPicker 2.0: Improved protein assembly with high discrimination peptide identification filtering. J Proteome Res. 2009; 8:3872–3881. [PubMed: 19522537]
51. Tabb DL, Friedman DB, Ham AJ. Verification of automated peptide identifications from proteomic tandem mass spectra. Nat Protoc. 2006; 1:2213–2222. [PubMed: 17406459]
52. MacLean B, et al. Skyline: an open source document editor for creating and analyzing targeted proteomics experiments. Bioinformatics. 2010; 26:966–968. [PubMed: 20147306]
53. Chambers MC, et al. A cross-platform toolkit for mass spectrometry and proteomics. Nat Biotechnol. 2012; 30:918–920. [PubMed: 23051804]
54. O'Shea JP, et al. pLogo: a probabilistic approach to visualizing sequence motifs. Nat Methods. 2013; 10:1211–1212. [PubMed: 24097270]

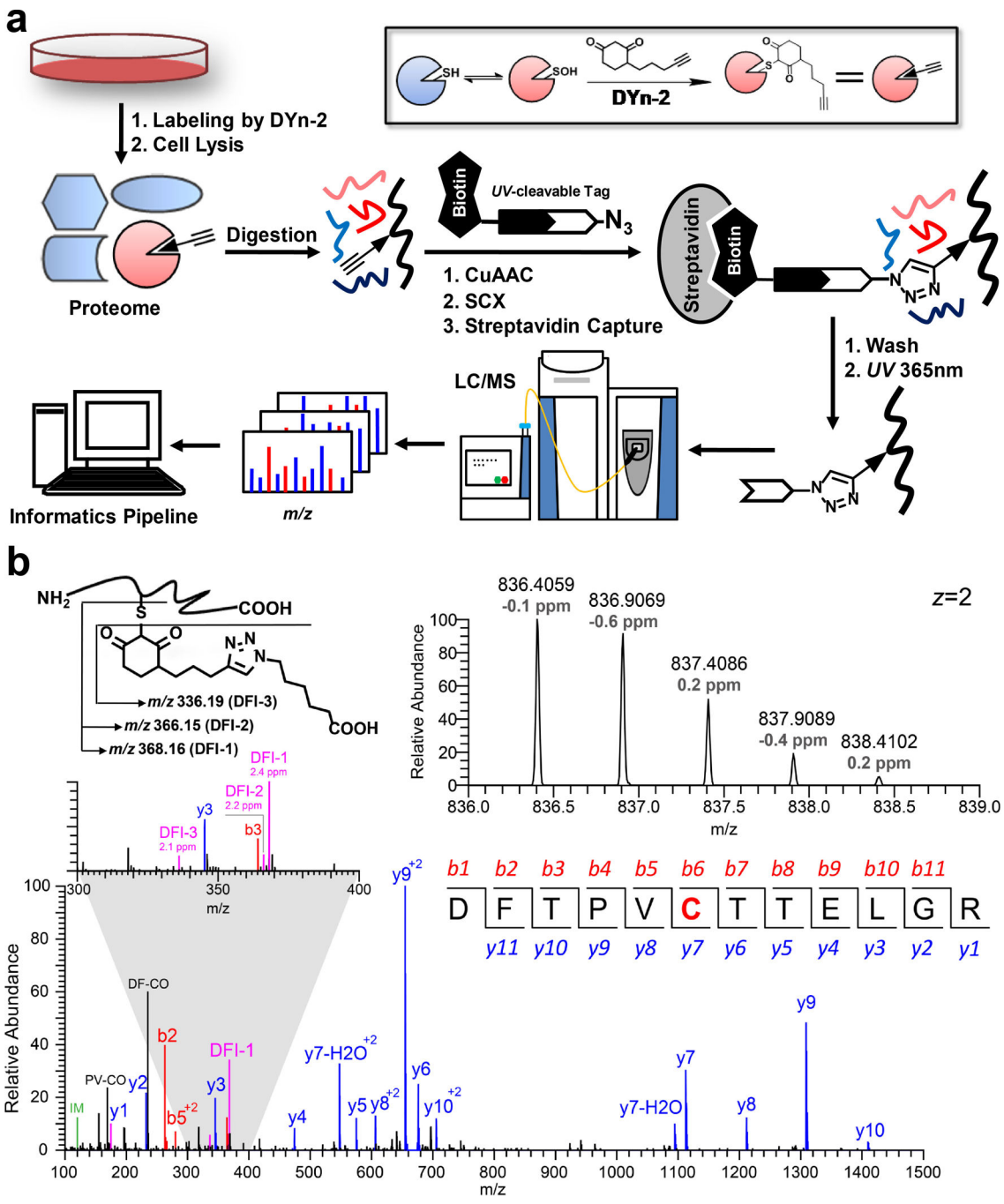


**Figure 1. Site-specific mapping of protein *S*-sulfenylation in cells**

(**a**) Workflow for selective labeling and analysis of protein *S*-sulfenylation in living cells. *S*-sulfenylated cysteines in intact RKO cells were labeled with the dimedone-based probe, DYn-2. Cell proteins then were digested with trypsin and labeled peptides were conjugated with azide biotin reagent, captured with streptavidin beads, and released by photocleavage of the biotin linker. The released DYn-2-triazohexanoic acid-modified peptides were analyzed by LC-MS/MS. (**b**) Characteristic fragmentation of modified peptides (upper, left) and a representative MS1 spectrum (upper, right) and HCD MS/MS spectrum (lower) of a

DYn-2-triazohexanoic acid-modified peptide from S-sulfenylated PRDX6. The highlighted cysteine in the peptide sequence represents the S-sulfenylated site (C47) of PRDX6. A zoom window displays the high mass accuracy of three diagnostic fragment ion (DFI) peaks.

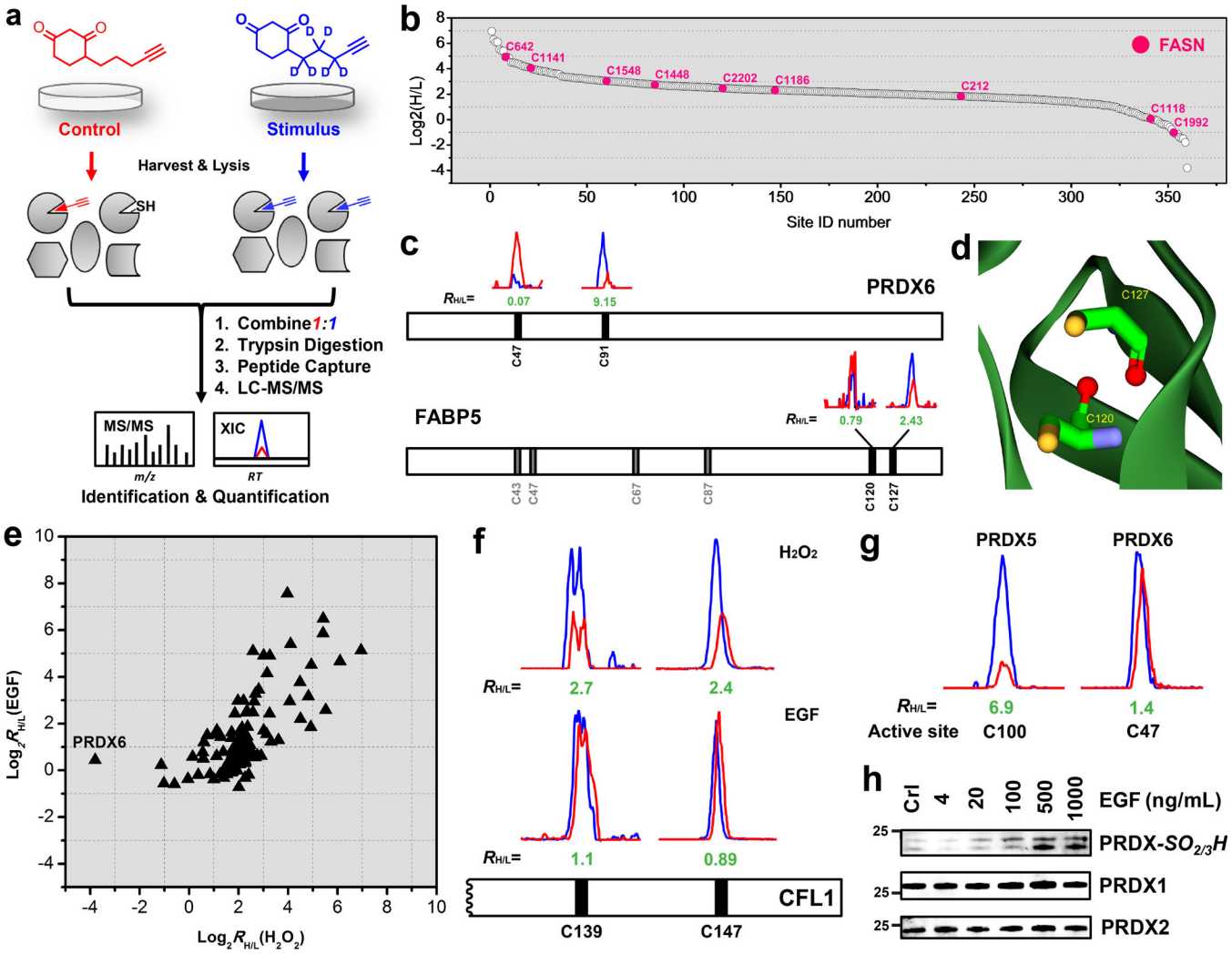


**Figure 2. Quantitative S-sulfenylome analyses in cells**

(**a**) Schematic representation of SulfenQ strategy. Intact cells treated with or without $H_2O_2$ were labeled with light and heavy DYn2, respectively, lysed and mixed at a 1:1 ratio for tryptic digestion and S-sulfenylated peptide capture. (**b**) The proteome-wide and site-specific changes in S-sulfenylation in intact RKO cells in response to exogenous $H_2O_2$ (500 μM, 5 min), where nine S-sulfenylated cysteines on the FASN protein are shown in red, and all other cysteines by white symbols. Ratios of heavy- to light- isotope labeled peak intensities ($H_2O_2$ vs control) are displayed on a log2 scale on the y axis. (**c**) Extracted ion chromatograms (XIC) are shown for changes in S-sulfenylated peptides from PRDX6 (top) and FABP5 (bottom) from $H_2O_2$ stimulation in RKO cells, with the profiles for light- and heavy- labeled peptides in red and blue, respectively. The site location and the experimental ratios calculated from at least four replicates are displayed below the individual chromatograms, respectively. (**d**) Two adjacent cysteine residues (C120 and C127, yellow color) were mapped onto the crystal structure of FABP5 (protein databank structure 4AZM). The structure was visualized using Discovery studio. (**e**) Analysis of S-sulfenylome changes induced by endogenous $H_2O_2$ production upon EGF stimulation and its correlation with that

produced by exogenous $H_2O_2$. $Log_2R_{H/L}$ values of the intensity of S-sulfenylated peptides identified using EGF (100 ng/mL, 5 min) as stimulus in A431 cells are plotted against those of data from $H_2O_2$ treatment, as shown in Fig.2b. Only peptides identified as S-sulfenyl sites in both datasets are included. (**f**) Comparison of XICs of S-sulfenylated peptides from CFL1 upon EGF and $H_2O_2$ treatment. (**g**) XICs of S-sulfenylated peptides from PRDX5 (2-Cys peroxiredoxin) and PRDX6 (1-Cys peroxiredoxin) upon EGF stimulation in A431 cells. (**h**) Levels of over-oxidized peroxiredoxins in A431 cells were treated with different concentrations of EGF for 5 min. Peroxiredoxins with the same catalytic sequence (PRDX1-4) were detected by immunoblotting using anti-peroxiredoxin-$SO_{2/3}H$ antibody. PRDX1 and PRDX2 were also immunoblotted as protein expression controls. Full-length gels are shown in Supplementary Fig. 11.

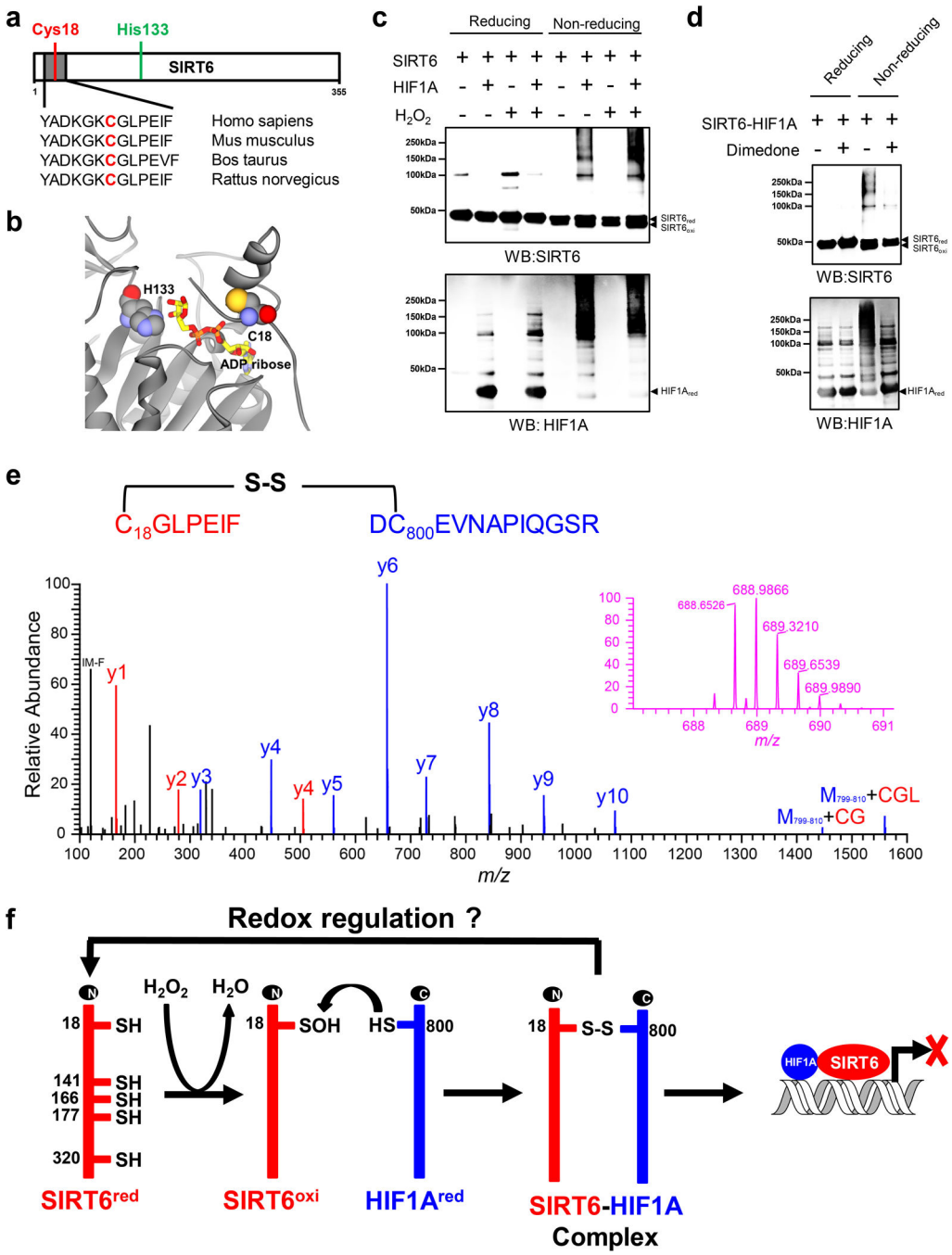


**Figure 3. Functional analysis of S-sulfenylation on SIRT6**

(**a**) The S-sulfenylation site Cys18 near the N-terminus of SIRT6 is evolutionarily conserved. (**b**) The S-sulfenylation site and the active site of SIRT6 were mapped onto the crystal structure of SIRT6 (PDB#: 3PKI) and visualized with Discovery Studio. (**c**) Human recombinant SIRT6 forms reducible, covalent complexes with HIF1A upon treatment with $H_2O_2$. Mixtures of the proteins were incubated with or without 0.5mM $H_2O_2$ at 37°C. After 4h incubation, the reaction mixtures were analyzed by reducing or non-reducing SDS-PAGE gels and SIRT6 (upper) or HIF1A (lower) complexes were detected by immunoblotting. (**d**)

Dimedone inhibits intermolecular disulfide formation between SIRT6 and HIF1A. $H_2O_2$ treated SIRT6-HIF1A mixtures were incubated in the presence or absence of 10 mM dimedone at 37°C for 4h and SIRT6 (upper) or HIF1A (lower) complexes were detected by immunoblotting. (**e**) Identification of the cysteines involved in the intermolecular disulfide formation between SIRT6 and HIF1A. Human recombinant SIRT6 and HIF1A fragment (530–826) were incubated with 0.5 mM $H_2O_2$ at 37°C. After 4h incubation, the reaction mixture was digested with trypsin and then with AspN and analyzed by LC-MS/MS. The MS/MS fragment ions of SIRT6 peptide (18–24) and HIF1A peptide (799–810) are depicted in red and blue, respectively. Inset shows the high resolution MS spectrum of the disulfide linked peptide from the SIRT6-HIF1A complex. (**f**) Hypothetical model for the redox-based gene regulatory interaction between SIRT6 and HIF1A.

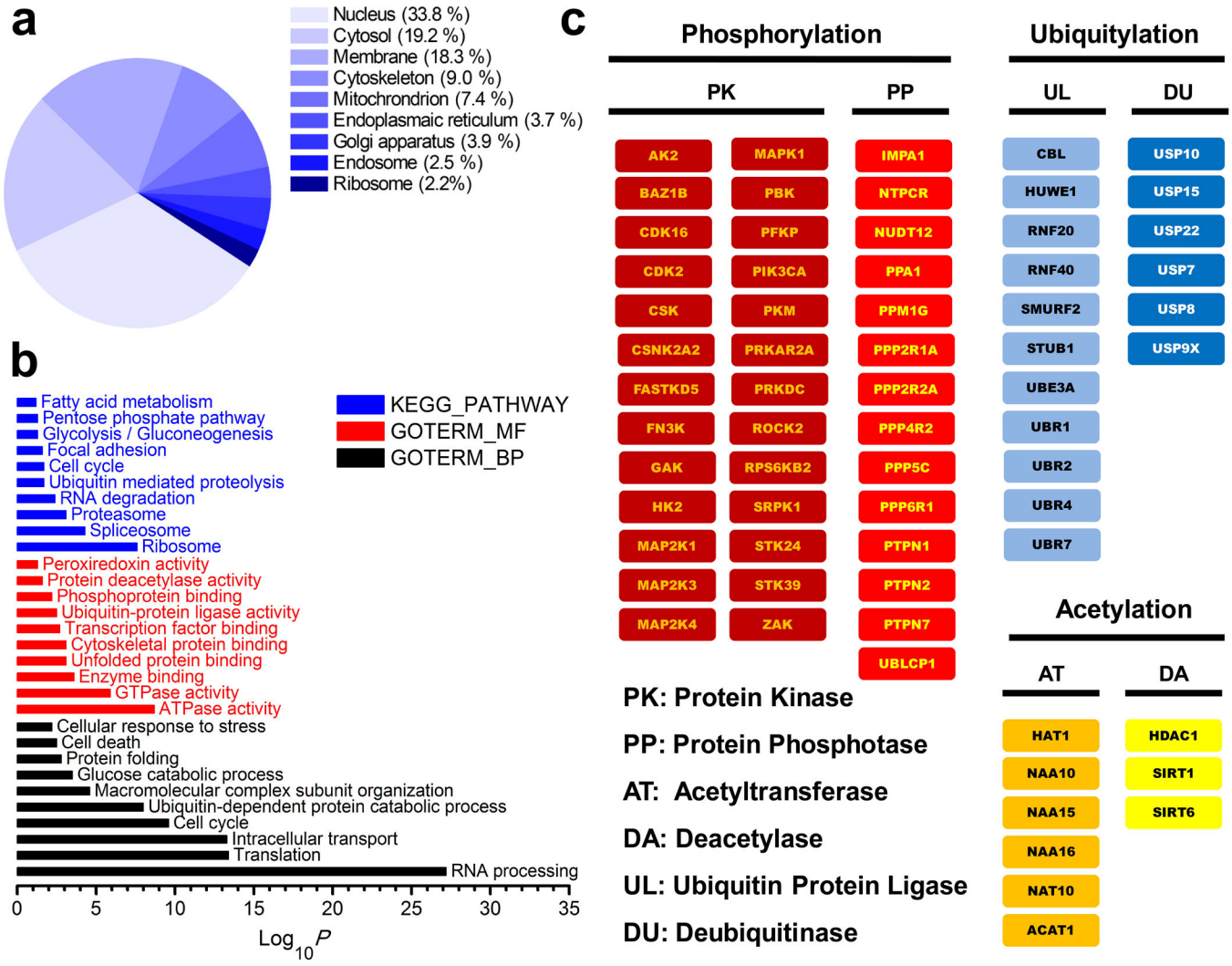


**Figure 4. Gene Ontology classification of the *S*-sulfenylome**

(**a**) Cellular compartment terms associated with sulfenylated proteins. (**b**) Gene Ontology annotations enriched in S-sulfenylome. (**c**) Occurrence of S-sulfenylation sites on proteins associated with posttranslational regulation of cell signaling.

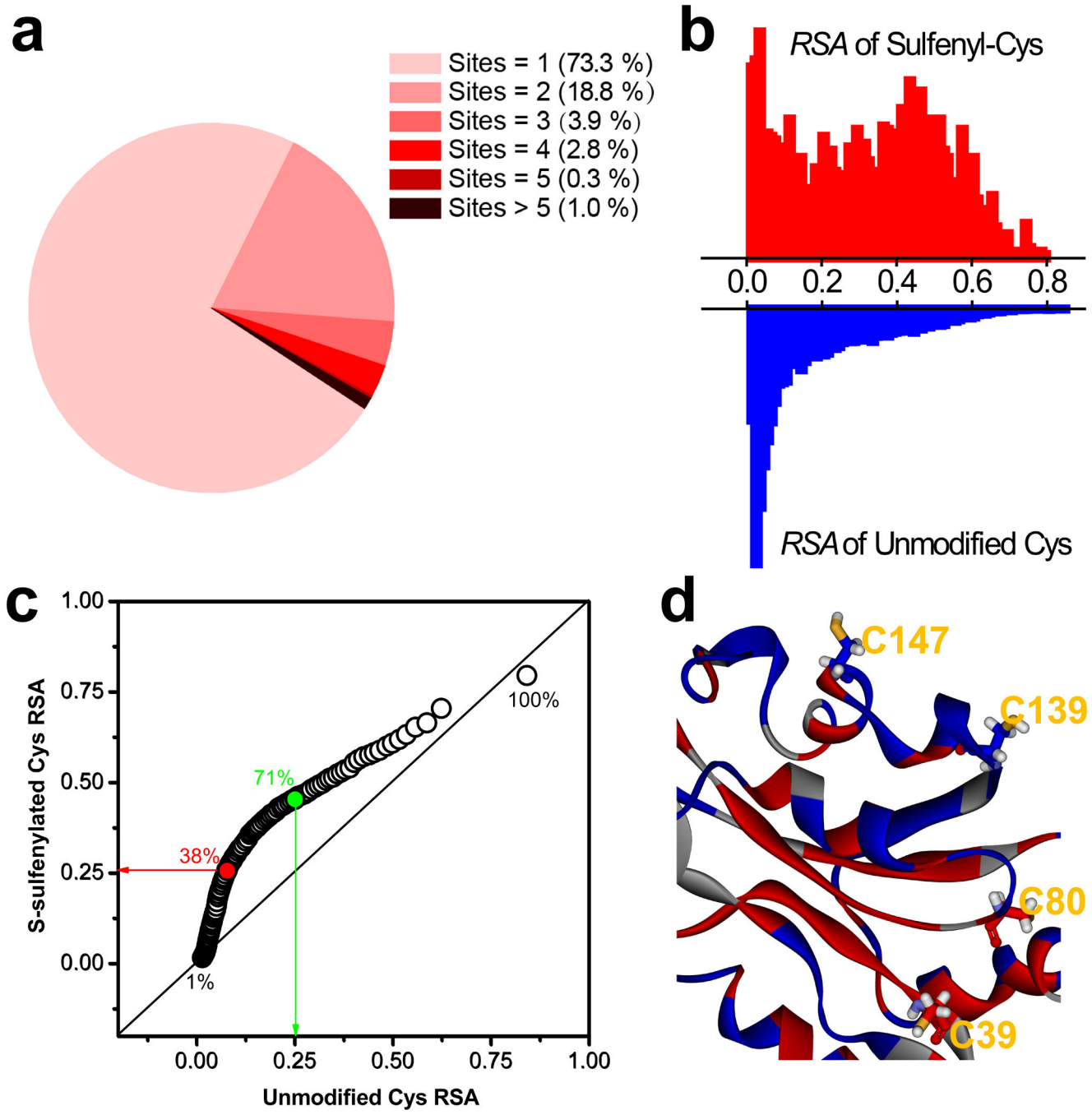


**Figure 5. Impact of cysteine surface accessibility on *S*-sulfenylation**

(**a**) Distribution of the number of *S*-sulfenylated cysteine residues per protein. (**b**) Distributions of the relative RSA for S-sulfenylated cysteine *versus* unmodified cysteine residues. (**c**) Q-Q plot of the relative RSA for S-sulfenylated cysteine *versus* unmodified cysteine residues. The relative RSA values of S-sulfenylated and unmodified cysteine residues were predicted with NetSurfP, percentiled and sorted from 1% to 100% with a 1% interval, respectively. The RSA values at the 38th percentile were 0.25 (S-sulfenyl) *versus* 0.08 (unmodified) and 0.45 (S-sulfenyl) *versus* 0.25 (unmodified) at the 71$^{st}$ percentile, thus

indicating that S-sulfenylated cysteine residues are favored at exposed protein surfaces. (**d**) Crystal structure of CFL1 (protein databank structure **1Q8G**) with the two S-sulfenylated cysteines (C139 and C147) mapped onto the solvent-accessible surface and the unmodified cysteines buried.

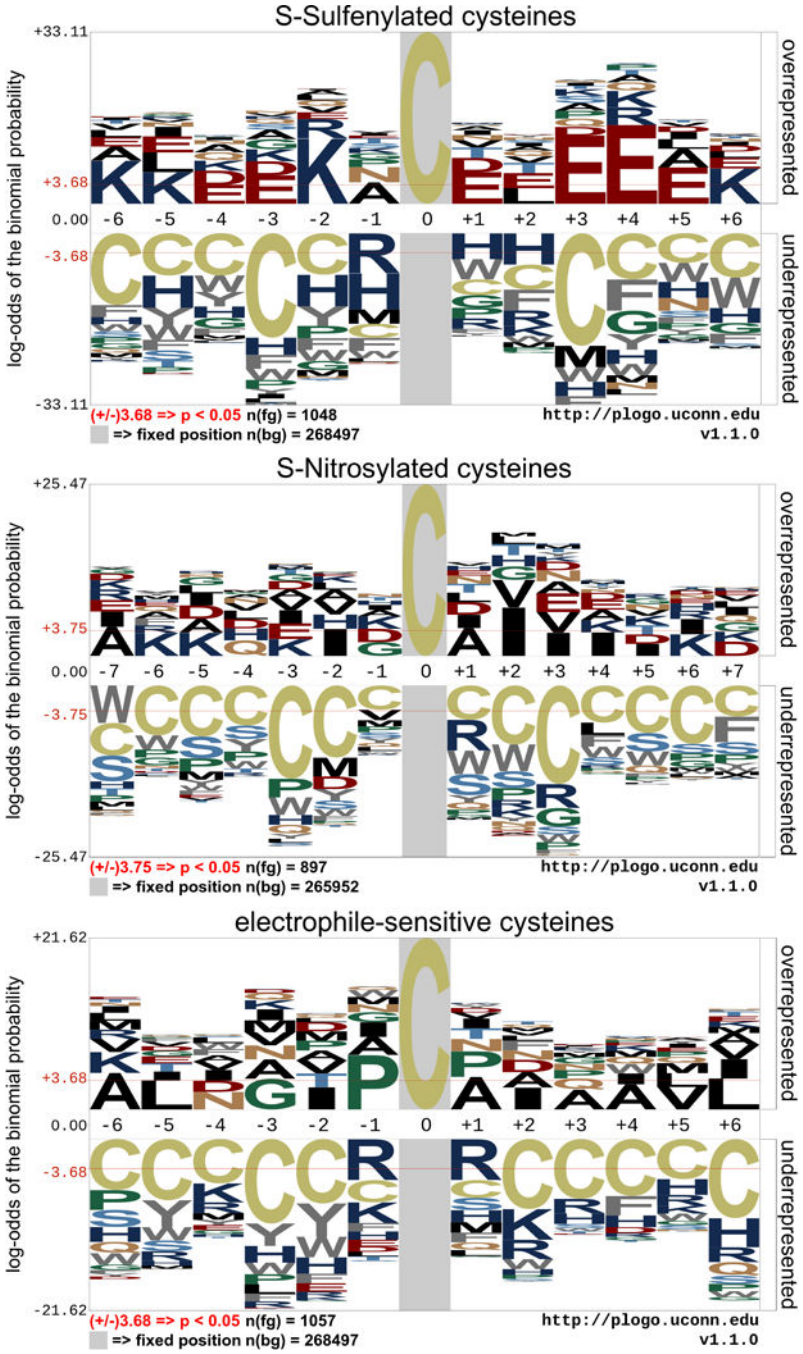


**Figure 6. Sequence motif analysis of protein S-sulfenylation**

Comparison of calculated sequence motif for S-sulfenylated (1048, human), S-nitrosylated (897, mouse) and electrophile-alkylated cysteines (1057, human). Images were generated with pLogo and scaled to the height of the largest column within the sequence visualization. The red horizontal lines on the pLogo plots denote p = 0.05 thresholds.